Talanta 107 (2013) 324–331

Contents lists available at SciVerse ScienceDirect

Talanta

journal homepage: www.elsevier.com/locate/talanta

Hydrogen peroxide biosensor based on microperoxidase-11 immobilized in a silica cavity array electrode

Shu Tian [a,b], Qun Zhou [a,*], Zhuomin Gu [a], Xuefang Gu [b], Lili Zhao [a], Yan Li [a], Junwei Zheng [a,*]

[a] College of Chemistry, Chemical Engineering and Materials Science, Soochow University, Suzhou 215123, PR China
[b] School of Chemistry and Chemical Engineering, Nantong University, Nantong 226007, PR China

ARTICLE INFO

Article history:
Received 10 November 2012
Received in revised form
13 January 2013
Accepted 17 January 2013
Available online 1 February 2013

Keywords:
Silica cavity
Microperoxidase-11
Modified electrodes
Hydrogen peroxide
Biosensor

ABSTRACT

Hydrogen peroxide biosensor based on the silica cavity array modified indium-doped tin oxide (ITO) electrode was constructed. An array of silica microcavities was fabricated by electrodeposition using the assembled polystyrene particles as template. Due to the resistance gradient of the silica cavity structure, the silica cavity exhibits a confinement effect on the electrochemical reactions, making the electrode function as an array of "soft" microelectrodes. The covalently immobilized microperoxidase-11(MP-11) inside these SiO_2 cavities can keep its physiological activities, the electron transfer between the MP-11 and electrode was investigated through electrochemical method. The cyclic voltammetric curve shows a quasi-reversible electrochemical redox behavior with a pair of well-defined redox peaks, the cathodic and anodic peaks are located at -0.26 and -0.15 V. Furthermore, the modified electrode exhibits high electrocatalytic activity toward the reduction of hydrogen peroxide and also shows good analytical performance for the amperometric detection of H_2O_2 with a linear range from 2×10^{-6} to 6×10^{-4} M. The good reproducibility and long-term stability of this novel electrode not only offer an opportunity for the detection of H_2O_2 in low concentration, but also provide a platform to construct various biosensors based on many other enzymes.

1. Introduction

The electrical contact between redox proteins and the electrode has attracted much interest, not only in fundamental studies about charge transfer properties of the redox proteins but also for further development of sensitive biosensors and bioelectronics devices [1–6]. Direct electron transfer (DET) is fundamental in fabricating a biosensor with high sensitivity and fast response. To achieve this, the redox protein must be immobilized on the electrode surface. Directly immobilizing a redox enzyme on the surface of a metal electrode or a metal nanoparticles modified (in particular gold nanoparticles) electrode are widely believed to be the most effective ways for enhancing the electron transfer (ET) between the enzyme and electrodes [7]. For example, microperoxidase-11(MP-11), as a hydrolytic digestion product of cytochrome *c*, consists of eleven amino acids with a covalently linked Fe III-protoporphyrin IX heme site [8]. Owing to the small size and relatively unshielded heme group, MP-11 could be the best candidate to serve as the core of a biosensor. However, MP-11 has been shown, in previous studies, to be electrochemically inactive at the bare gold electrode [9]. Consequently, over the past two decades, great efforts have been devoted towards the development of immobilization procedures to promote DET and bioelectrocatalytic activity. The binding of redox enzymes to the conducting nanostructures is accomplished through several methods, such as chemisorption via thiol groups, electrostatic adsorption by modifiers, or coupling by bifunctional reagents to surface functionalities [10–14] Lötzbeyer and Schuhmann pioneered the immobilization of MP-11 onto the gold surface [15,16]. They demonstrated that direct and fast electron transfer could occur when MP-11 was covalently immobilized on the cystamine modified gold electrode, which was also confirmed by Jiang et al. using 3-mercaptopropionic acid to bind MP-11 [17]. In these papers, the self-assembled monolayers (SAMs) technique was utilized to immobilize enzymes via a covalent link to sulphur-containing compounds chemisorpted on a conductive substrate. With the usage of these "flexible" mediators (owing to the easiness of preparation and the possibility of changing the alkyl chain length and the functional terminated group) [18], small molecules (usually O_2, H_2O_2) in the electrolyte solution can diffuse in and react with the active centre of the enzyme immobilized on the organosuphur molecule and then react with the electrode surface; thus, ET between the enzyme and the electrode is achieved [19]. In addition, previous researches have revealed that the distances between electrodes can be greatly reduced when electrochemical reactions occur in a very small volume, resulting in the overlap or coupling of two diffusion layers in the electrodes; therefore, high signal intensities and optimal signal-to-noise ratios can be

* Corresponding authors. Tel.: +86 512 6588 0362; fax: +86 512 6588 0089.
E-mail addresses: zhq@suda.edu.cn (Q. Zhou), jwzheng@suda.edu.cn (J. Zheng).

0039-9140/$ - see front matter © 2013 Elsevier B.V. All rights reserved.
http://dx.doi.org/10.1016/j.talanta.2013.01.050

achieved under ambient analyte conditions [20–22]. Thus, it is reasonable to expect that if MP-11 is placed into a micro or nanoreactors to fabricate a kind of microelectrode (at least microcathode), we might obtain a novel biosensor with fast response and high sensitivity.

Microreactors provide a microenvironment for chemical reactions to occur inside it and acts as a microdevice for material and energy conversion [23], which gives us an approach that enables a chemical reaction to be studied on a molecular level. There are several methods for fabricating micro or nanodevices, such as lithographic methods, nano-imprinting and scanning probe microscope (SPM) writing techniques [24,25]. However, the relatively high cost of these facilities is beyond the purchasing power of most laboratories. Compared to lithographic methods and SPM writing processes, template-based methods are time-saving approaches with low equipment cost for preparing surface nanostructures [26]. A general method for fabricating bowl-shaped nanovoid architectures was introduced by Velev et al. [27,28], and has been well-developed by the same group and many other groups [24,29–34]. With highly ordered monodispersed nanoparticles (usually silica and PS particles) as a template, functional materials can be deposited into the interspace of the template particles. Cavities that are opened at both the top and bottom are obtained after the template is removed, with the same shape and size as the template. To a certain extent, microelectrodes can be fabricated on the condition that the micro or nanovoids were arranged on a conductive substance; the nanobowls may then be used as ultrasmall containers for holding fluids at nanoscale volumes. The species in the solution are provided direct access, through the open pore and exposed bottom, to the underlying surface.

In this paper, we report a novel hydrogen peroxide biosensor based on a silica cavity array electrode. A two dimension array of hemispherical silica cavities, opened at top and bottom, was fabricated on the surface of ITO electrodes using 2 μm diameter polystyrene (PS) as the template, and followed by the electrochemical deposition of gold nanoparticles (GNPs) at the bottom of the cavities. A monolayer of 4-mercaptobenzoic acid (MBA) was then attached to the GNPs through S–Au bond, and acted as a mediator to covalently immobilize MP-11. Scanning electron micrographs (SEM), electrochemical impedance spectroscopy (EIS) and cyclic voltammetry (CV) were employed to characterize and delineate the electrochemical performance of this novel electrode. It was found that the SiO_2 cavity provided a favorable microenvironment for MP-11 to achieve its direct electron transfer and to maintain its electrocatalytic activities. The electrocatalytic performance of the modified electrode to hydrogen peroxide was also investigated.

2. Experimental section

2.1. Materials and apparatus

Microperoxidase-11 was purchased from Sigma-Aldrich, 1-ethyl-3-(3-dimethylaminopropyl) carbodiimide (EDC), *N*-hydroxysucinimide (NHS), 4-mercaptobenzoic acid and polyvinylpyridine (PVP), tetramethoxysilane (TMOS) were purchased from J&K (Japan). A fresh solution of H_2O_2 was prepared before being used. The supporting electrolyte was 0.1 M KH_2PO_4/K_2HPO_4 phosphate buffers solution (pH 6.0–8.0). Polystyrene (PS) particles were synthesized by a dispersion polymerization of styrene in ethanol–water mixtures according to literature [35]. Ultrapure water used in washings and all buffer solutions preparations was produced in Millipore-*Q* system.

The SEM were observed on a Hitachi S4700 (Japan) field emission scanning electron microscope. Cyclic voltammograms (CV) and electrochemical impedance spectroscopy (EIS) were recorded on a CHI 660D electrochemical station (Shanghai Chen-Hua Instruments CO LTD., China). A bare or modified ITO electrode was employed as the working electrode. In order to maintain the constant surface area of the working electrode, the surface of the electrode was sheltered by a sticker, only a circular portion of 0.5 cm diameter was exposed to the solution. A platinum and an Ag|AgCl (saturated KCl) electrode were used as the auxiliary and reference electrodes, respectively. All electrochemical measurements were conducted in argon-purged (at least 30 min and kept under an argon atmosphere during whole course) solution and at room temperature.

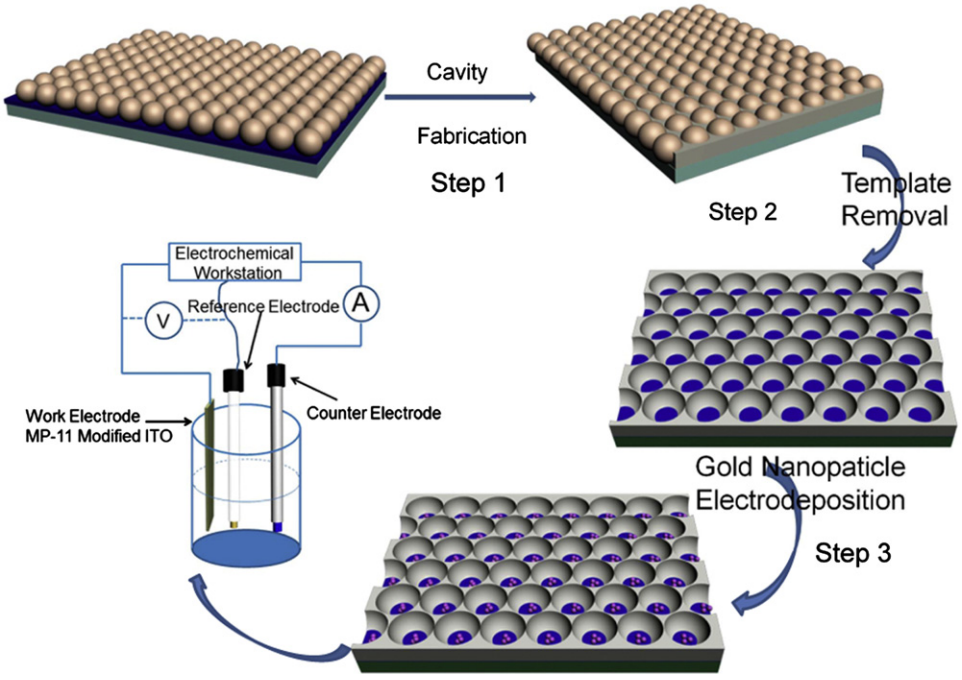

Scheme 1. Schematic illustration of the procedures for fabricating the MP-11 modified electrode and the conventional three-electrode system..

2.2. Preparation of modified electrodes

2.2.1. Preparation of ordered microcavities

The fabrication of the silica cavity modified ITO is schematically illustrated in Scheme 1. For the fabrication of highly ordered PS sphere template, 0.5 mL water/ethanol containing monodisperse PS spheres (5 wt%) was injected slowly onto the surface of Millipore-Q water in a Petri dish, the PS spheres spread freely over the top surface of water until it covered nearly the whole surface area. A few drops of 2 wt% SDS solution were then added onto the water surface to lower the surface tension and to make the PS spheres closely packed. The whole system was kept under an environment free from outside disturbance to sedimentate the suspended PS particles in the water for 24 h. Then the close packed PS particles were transferred onto the surface of an ITO electrode and dried at 110 °C for 1 h, this was done to remove the remaining solvent in the monolayer and generate a highly ordered template structure of the close-packed PS particles. Silica was electroplated through the templates from a sol–gel bath. A typically composition of the plating solutions contains 5 mL of 0.2 M KCl, 5 mL of ethanol, 1 mL of TMOS and 0.6 mL of 0.1 M HCl. For preparation, the solution was left under continuous stirring for 1 h at room temperature before the addition of 50 mM H_2O_2. Potentials in the range of −0.4 to −0.8 V were applied to the working electrode for a period of 5–30 min. After that, the electrode was taken out of the cell, rinsed softly with water, and dried overnight at a relative humidity of 35%, room temperature (Scheme 1 step 1). Then the electrode was immersed into toluene to dissolve the PS spheres, leaving an ordered array of interconnected sphere segment voids (Scheme 1 step 2). The obtained structured silica spherical cavities were robust and adhered well to the ITO electrode.

2.2.2. Immobilization of MP-11

The electrodeposition of GNPs on the bottom of silica cavities was performed potentiostatically at −0.9 V in a 0.1 M KNO_3 solution containing 1 mM $HAuCl_4$ for 40 s (Scheme 1 step 3). The structured ITO electrode was then rinsed twice with water and modified with MBA by soaking into a 10 mM solution in ethanol for 4 h at room temperature. The freshly prepared electrode was rinsed with water and incubated in 100 mM EDC and 50 mM NHS pH 6.0 PBS for 6 h at room temperature to activate the terminal carboxylic group of MBA. Subsequently, the electrode was rinsed thoroughly and immersed into 1 mg/mL MP-11 pH 7.0 PBS at 4 °C overnight. Finally, the electrode was copiously rinsed with water and dried in a jet of argon and stored at 4 °C.

Additionally, physisorption of Au nanoparticles on bare ITO electrode was according to the following protocol: an ITO electrode was immersed in a saturated PVP ethanol solution for 24 h to form a positive charged surface, after being completely washed with ethanol and water, the ITO electrode was then immersed in a colloid solution of the GNPs for 12 h. After that, the surface of the ITO was covered with a monolayer of the GNPs. Immobilization of MP-11 on the result electrode was the same as the procedure mentioned above.

3. Results and discussion

3.1. Preparation and characterization of ordered microcavities

The PS particles can be spontaneously assembled into a 2-D monolayer with a large area at the air/water interface, due to the lateral capillary force and convective flow, resulting from an imbalance in the surface force arising from differences in the curvature of the liquid surface and the evaporation of the liquid, respectively. As the monolayer of PS particles is transferred onto the surface of the ITO electrode, the highly ordered assembly structure of the PS particles can be preserved. The SEM image of the PS particles assembled on the ITO electrode is shown in Fig. 1a. It can be seen that the PS particles are well assembled into

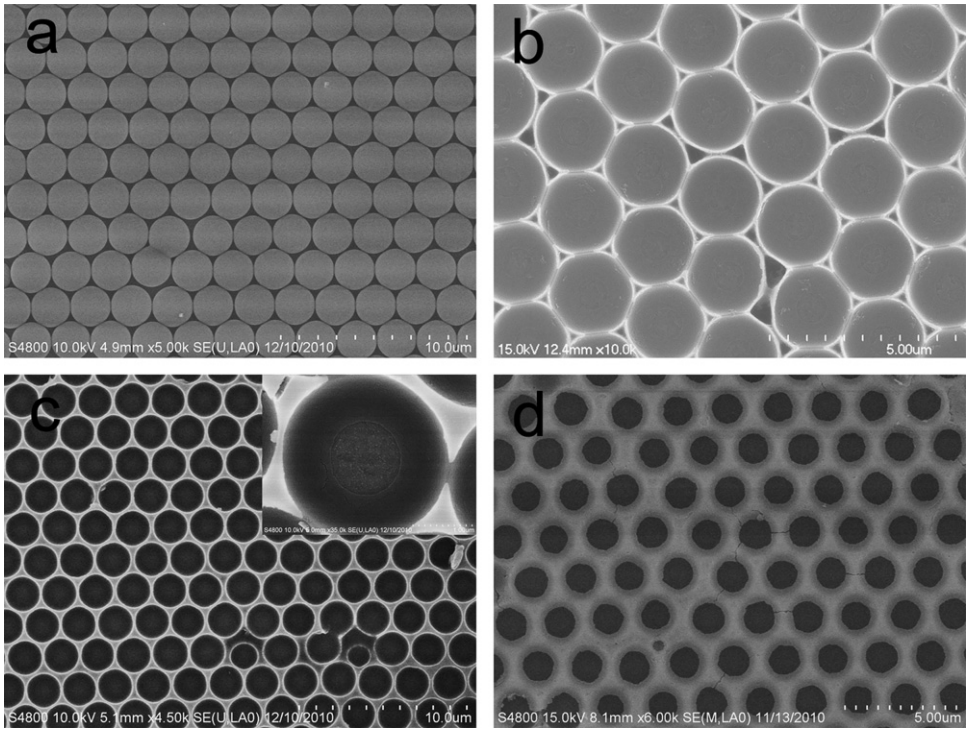

Fig. 1. SEM images of (a) ordered PS particles and the silica cavities array formed at different electrodeposition times (b) 5 min and (c) 15 min and (d) 30 min. The inset of (c) is a blowup of single cavity.

a close-packed two-dimensional structure. Silica cavities were formed by electrodeposition using the highly ordered PS particles as the template. In a H_2O_2-containing solution, H_2O_2 can be reduced to generate OH^- ions at a proper potential on the electrode surface. The resulting OH^- ions consequently catalyze the hydrolysis of the alkoxysilane (TMOS in this work) to form the silica at the ITO electrode surface. The advantages of the electrodeposition method for the formation of the silica cavities include: (1) the silica film uniformly grows at the surface of the ITO electrode, ensuring the high quality of the silica cavities because no silica could be coated at the top of the PS particles during the first stage of the electrodeposition; (2) the depth of cavities can be easily controlled through the electrodeposition parameters, such as deposition time, potential and ingredient of the electrolyte. Fig. 1b–d display the SEM images of the silica cavities formed on the surface of ITO electrodes at −0.6 V. As the deposition time was less than 5 min, the interspaces among the PS particles were only partially filled with silica (Fig. 1b), resulting in the exposure of the underlying ITO surface at interstice among the cavities. Prolonging the deposition time to 15 min led to a complete formation of the semispherical silica cavities (Fig. 1c). The arrangement of the silica semispherical cavities exactly reflects the assembled structure of the PS particles. As the electrodeposition time was more than 30 min, a further increase in the depth of the cavities was observed (Fig. 1d). The extra amount of SiO_2 deposited under this circumstance resulted in a decrease in the size of the opening of the cavities. It is important to note that the bottom of the cavities was not fully covered with SiO_2, a magnified SEM graph of a single cavity suggested that a defect site with a diameter of 600 nm was formed in each cavity (inset of Fig. 1c). Therefore, the surface of the ITO electrode is exposed at the bottom of the SiO_2 cavities.

To verify the accessibility of the silica cavity to an electrochemical reaction, the electrodeposition of gold metal was performed with the silica cavity-modified ITO electrode in a solution containing 1 mM $HAuCl_4$. The reduction of the Au complex-ion was carried out at −0.9 V vs. Ag/AgCl. A SEM image of the electrode after the gold deposition was taken and the result is shown in Fig. 2. As can be seen, the nano-sized gold particles were uniformly deposited at the bottom of the cavities. No gold particle grew on the outer surface of the cavities. This result demonstrates that the electrochemical reaction is limited to inside the cavities and occurs only at the bottom of each silica cavity.

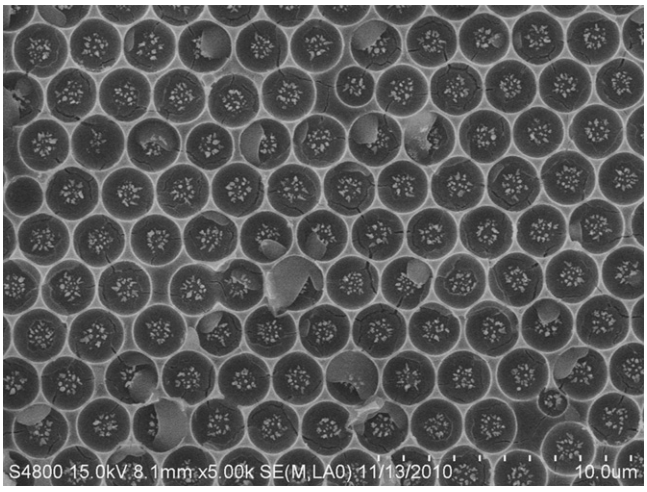

Fig. 2. SEM image of silica cavity array after GNPs electrodeposition.

3.2. Preparation and characterization of modified electrodes

MP-11, an excellent electrochemical catalyst for the reduction of hydrogen peroxide, was tentatively selected to functionalize the GNPs inside the silica cavities on the ITO electrode: so that the bioelectrochemical reaction of the MP-11 molecules could occur in a confined volume at the microliter level. In order to immobilize the MP-11 molecules onto the GNPs, in this case, the surface of the GNPs is first modified with the MBA molecules, which in turn, serve as the linker between the MP-11 molecules and the GNPs. That is, the thiol group of the MBA molecules is attached to the GNPs through the formation the surface Au–S covalent bond, the carboxylic group of the MBA molecules, on the other hand, can be crosslinked with the ammo acid residues of the MP-11 molecules under the activation of the EDC molecules.

3.2.1. UV–vis absorption spectra

It is well-known that GNPs display surface plasmon resonance (SPR) bands in the visible spectral region. Fig. 3 shows typical UV–vis spectra for GNPs at different stages of modification. The SPR of immobilized GNPs occurred at 545 nm (Fig. 3a) with a relatively broad peak, corresponding to the aggregation of the GNPs resulting from interparticle interactions adsorbed on the electrode surface [36], which was consistent with SEM observations. After chemisorption of the MBA molecules to the surface of nanoparticles, a red shift to 561 nm together with a small broadening of the SPR band in the long wavelength region was observed (Fig. 3b). In general, the locations of the dipolar and quadrupolar modes of the SPR strongly depend on the shape, size and the environment of the metal nanoparticles [37]. In this case, the red shift of the SPR band upon the adsorption of the MBA molecules likely resulted from a change in the dielectric property of the media surrounding the GNPs. A further shift of the SPR band to 578 nm was observed after the immobilization of the MP-11 molecules. In addition, new bands appeared at ca. 408 and 535 nm, corresponding to the characteristic Soret-band and Q band of MP-11, respectively (Fig. 3c). This Soret-band has been attributed to the π–π^* transition of the porphyrin cycle in the heme group of the MP-11 molecule [38], and the similarity of the Soret-band for the immobilized and the free MP-11 molecules indicates that no evident structure alteration of the MP-11 molecules occurs during the immobilization process.

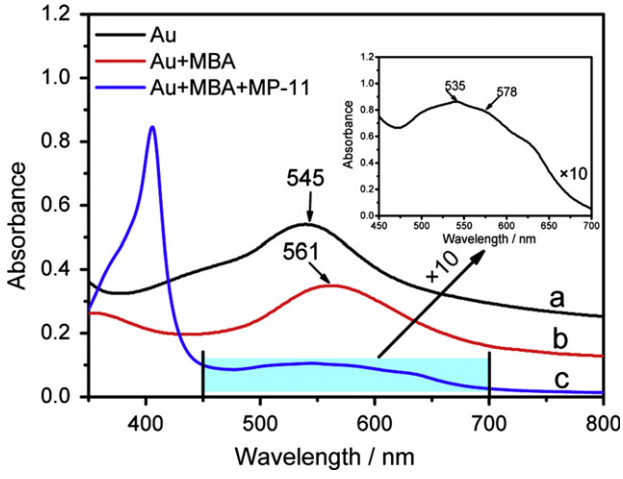

Fig. 3. UV–vis spectra of (a) Au/SiO_2 cavity modified ITO electrode, (b) MBA/Au/SiO_2 cavity modified ITO electrode, (c) MP-11/MBA/Au/SiO_2 cavity modified ITO electrode. Inset is a partial enlarged detail of curve c. (For interpretation of the references to color in this figure legend, the reader is referred to the web version of this article.)

3.2.2. Electrochemical impedance spectroscopy (EIS) of the modified electrode

In order to characterize the interfacial features of ITO electrodes during the modification process, EIS were performed at 0.2 V in a phosphate buffer (pH 7.0) solution containing 0.1 M KNO_3 and 5 mM $Fe(CN)_6^{3-/4-}$; the results are shown in Fig. 4A. The electron transfer resistance (R_{et}) values of the ITO surface before and after the modification of the silica cavity were estimated to be 23 (curve a) and 275 Ω (curve b), respectively. Then the GNPs were electrodeposited at the bottom of the silica cavities. It was found the diameter of the semicircle decreased, and the R_{et} value was estimated to be 54 Ω (curve c), indicating an effective improvement in the heterogeneous electron transfer kinetics between the redox couple and electrode interface. However, the R_{et} value increased to 138 Ω after the MBA molecules were adsorbed on the GNPs (curve d), which could be attributed to electrostatic repulsion due to the negatively charged COO^- and $Fe(CN)_6^{3-/4-}$. As for the MP-11/MBA-Ag-cavities/ITO electrode (curve e), the R_{et} value was further increased to ca. 187 Ω, confirming the successful immobilization of MP-11 on the surface of the electrodes.

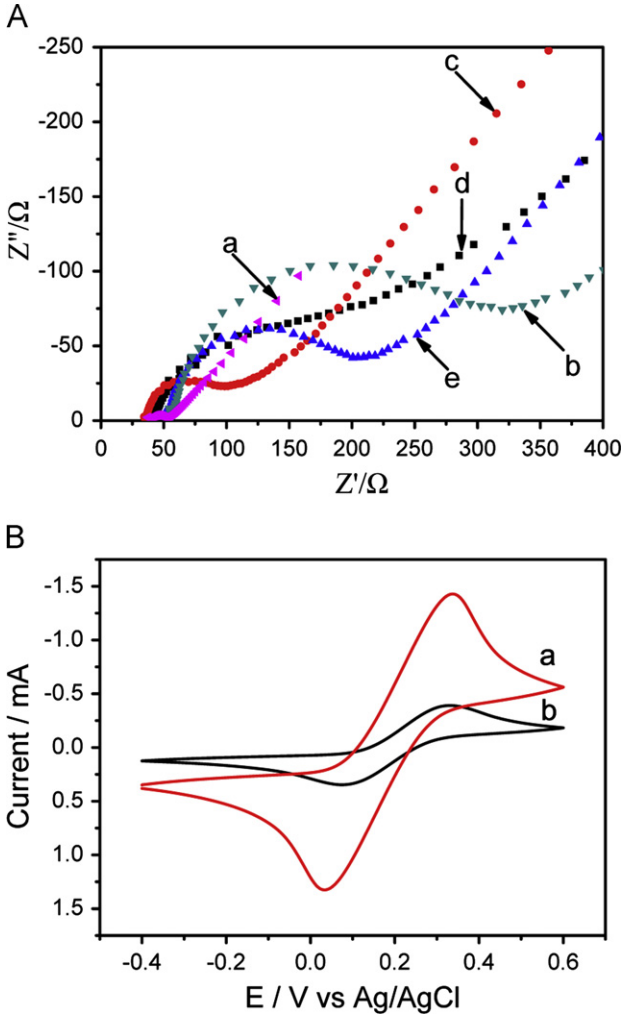

Fig. 4. EIS and CVs of different electrodes in the presence of 0.1 M KNO_3 solution with 5 mM $Fe(CN)_6^{3-/4-}$. (A) Nyquist plots of: (a) SiO_2 cavity modified ITO electrode, (b) Au/ITO with cavities, (c) MBA/Au/SiO_2 cavity modified ITO electrode and (d) MP-11/MBA/Au/SiO_2 cavity modified ITO electrode. The applied electrode potential was 0.20 V vs. Ag|AgCl, frequency range was 100 kHz–5 mHz. (B) Cyclic voltammograms obtained on (a) bare, (b) SiO_2 cavity modified ITO electrodes. Scan rate: 100 mV/s.

3.2.3. Confinement effect of the SiO_2 cavities on electrochemical reactions

Due to the low conductivity of SiO_2 and the exposure of the bottom of the cavities, it is expected that the bottom part of each SiO_2 cavity should be the favorable pathway for the electron transfer from the ITO electrode to the species in solution, thus the electrochemical reaction occurred in a confined volume, resulting in a faster mass transfer and electron transfer process. To verify this point, the cyclic voltammetric responses of 5 mM $Fe(CN)_6^{3-/4-}$ in 0.1 M KNO_3 solution were examined on the bare ITO and the silica cavity modified ITO electrodes; the results are shown in Fig. 4B. On the bare ITO electrode (curve a), a pair of anodic and cathodic peaks at 0.338 and 0.035 V, respectively, was observed, corresponding to the reversible redox reaction of the $Fe(CN)_6^{3-/4-}$ couple. While on the SiO_2 cavity-modified electrode the anodic peak shifted to 0.324 V and the cathodic peak shifted to 0.078 V (curve b). That is, the modification of the SiO_2 cavities on the electrode surface results in a reduction in the potential separation between the anodic and cathodic peaks, indicating an acceleration in electron transfer. This observation is very similar to our previous report on a ZnO cavity modified ITO electrode [39]. Moreover, the CV of the $Fe(CN)_6^{3-/4-}$ couple shows definite anodic and cathodic currents, giving a sigmoidal shaped I–E curve, indicating the predominance of radial diffusion to electrode surface [40]. To a certain extent, the CV behavior is similar to that for the array of microelectrodes in that there is some overlap of the individual diffusion layers, as indicated by the non-steady-state current and a hysteresis between the forward and backward scans [30]. The results also fit well with the characteristics of the microelectrode in low current, a small *iR* drop and fast response [41]. It seems to indicate that the resistance gradient of the SiO_2 cavities and the specific shape confinement of the electrochemical reaction zone make the ITO electrode function as an array of "soft" microelectrodes.

3.3. Direct electrochemistry of the modified electrode in PBS

The direct electrochemistry of MP-11 further demonstrated that as-prepared "soft" microelectrodes can accelerate the DET between the electroactive center of MP-11 and the electrode surface. Typical cyclic voltammograms (CVs) of the bare ITO and modified electrodes with and without MP-11 adsorbed on the surface of the electrodes are shown in Fig. 5. No redox peak was observed at the bare ITO, Au/ITO (figures not given), and MBA/Au ITO electrodes in 0.1 M PBS (pH 7.0) with 0.2 mg/mL MP-11 (curve a), indicating that direct electron transfer of MP-11 on these electrodes was too slow to be observed. For the MP-11 immobilized on the MBA/Au/SiO_2 cavity modified ITO electrode (curve c), a pair of well-defined redox peaks clearly appeared, in the potential region between −0.5 and 0.1 V, corresponding to the direct electron transfer between the heme active site of MP-11 and the electrode surface. The cathodic and anodic peaks are located at −0.26 and −0.15 V, respectively, The peak-to-peak separation ΔEp=Epa−Epc=110 mV, and the ratio of the anodic peak current to the cathodic Ipa/Ipc was 0.92 ± 0.02, suggesting a quasi-reversible one-electron electrochemical reaction for the immobilized MP-11 molecules. For the electrode without modification of the SiO_2 cavity, the cathodic and anodic peaks for the MP-11 immobilized on it are −0.28 and −0.08 V, respectively (curve b). The peak potential separation is about 200 mV and the peak current is significant lower than that at the MBA/Au/SiO_2 cavity modified ITO electrode. The result suggests that the MP-11 molecules also undergo a quasi-reversible electrochemical reaction, but with increased irreversibility. In this case, we estimate the apparent surface coverage of the SiO_2 cavity (θ) according to $\theta = 1 - R_{et}/R_{et}'$, where R_{et} and R_{et}' represent the electron transfer

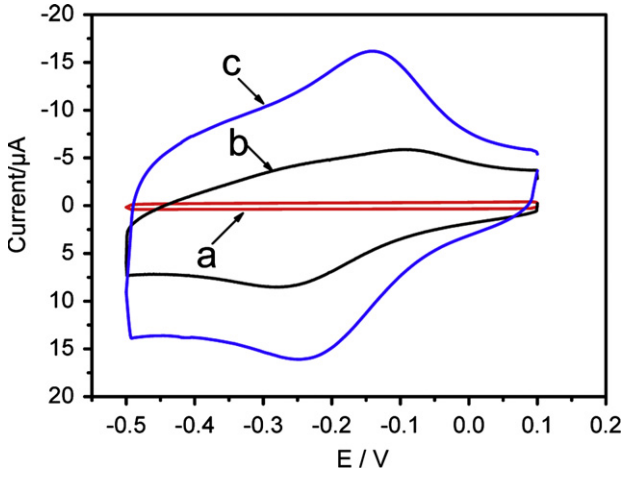

Fig. 5. Cyclic voltammetric curves of (a) MBA/Au ITO electrode in pH 7.0 PBS containing 0.2 mg/mL MP-11, (b) MP-11covalently attached to MBA without and (c) with silica cavities on ITO electrode in pH 7.0 PBS at scan rate 100 mV/s.

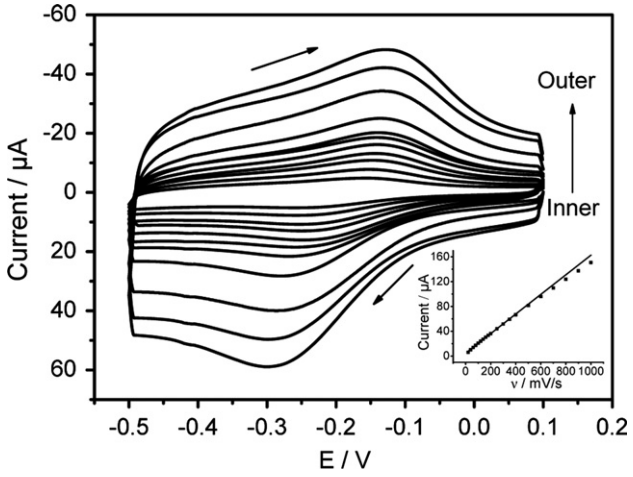

Fig. 6. Effect of scan rate on the CVs of MP-11 modified electrode in pH 7.0 PBS (from inner to outer curves: 20, 40, 60, 80,100, 120, 140,200, 250, 300 and 350 mV/s). Inset: Plot of peak current vs. scan rate from 20 to 1000 mV/s.

resistance of electrode before and after SiO_2 cavity modification, respectively. Thus, the coverage of SiO_2 cavity is calculated to be $\theta_{SiO_2}=1-R_{et}/R_{et'}=1-23/275=92\%$, which means there is only 8% effective electrode area available for the electrochemical reactions on the modified electrode. Consequently, the acceleration of the electron transfer and the increase of the redox current should not be simply explained by the influence of surface area and unique electrical conductivity of the GNPs. As the only difference between the two electrodes is the structure of the deposited SiO_2 cavity, it is reasonable to attribute the faster electron transfer to the contribution of SiO_2 cavity, due to its confined volume for electrochemical reaction.

The surface coverage of the electroactive substance was calculated according to the Laviron equation [42],

$$I_p = n^2F^2A\Gamma\nu(4RT)^{-1} = nFQ\nu(4RT)^{-1}$$

where I_p represents the anodic or cathodic peak current, Γ is the surface coverage of the electroactive substance (mol/cm^2), ν is the scan rate, A is the electrode area (cm^2, in this case, it is $\pi r^2=3.14\times(0.5/2)^2=0.2$ cm^2) and Q is the quantity of charge (C) calculated from the peak area of the voltammograms, n is the number of electron transferred. F is the Faraday constant; R is the gas constant; T is the absolute temperature. In our present work, the I_p at 100 mV/s scan rate was about 3.1 μA, the quantity of charge transferred Q was estimated to be 2.81×10^{-6} C, then n was calculated to be 1.09 (which is almost similar to the theoretical value). The amount of adsorbed MP-11 was calculated to be 1.34×10^{-10} mol/cm^2.

Fig. 6 shows the CVs of the MP-11/MBA/Au/SiO_2 cavity modified ITO electrode in PBS at various scan rates. The peak potential separation increases with scan rate ranging from 20 to 350 mV/s; however, the formal potential remains constant (−0.21 V). The inset in Fig. 6 shows the linear dependence of peak current on scan rate from 20 to 1000 mV/s. As can be seen, the peak currents rise linearly with an increase in the scan rate in the range from 20 to 500 mV/s, which indicates that the electron transfer of the MP-11 molecules was a surface-confined process.

Moreover, only a slight increase in the potential separation of the cathodic and anodic peaks was observed, implying a fast electron transfer rate for the immobilized MP-11 molecules on the electrode. The relationship between the cathodic peak potential and the scan rate follows Laviron's equation [42,43].The relationship between the peak potentials (Epc and Epa) and the natural logarithm of the scan rate (ln ν) for MP-11 on this type of modified electrode in 0.1 M PBS

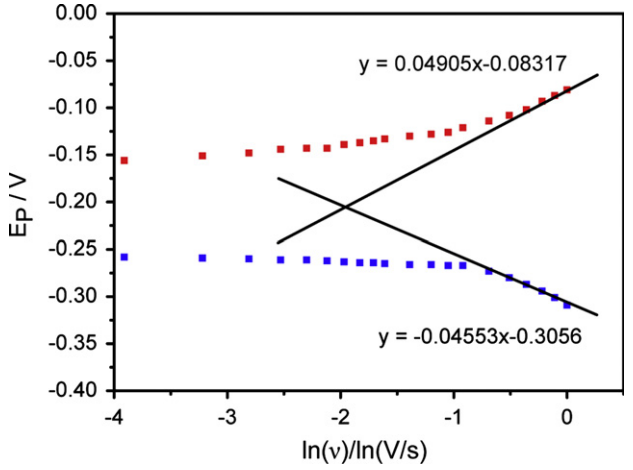

Fig. 7. Relationship between the peak potential (Ep) and the natural logarithm of scan rate for MP-11/MBA-Au-cavities/ITO electrode in pH 7.0 PBS.

(pH 7.0) are shown in Fig. 7. As can be seen, in the range from 0.5 to 1 V/s, the Epc and Epa change linearly versus ln ν with linear regression equations of $y=-0.04553x-0.3056$ and $y=0.04905x-0.08317$, respectively; αn is calculated to be 0.58 (α and n corresponding to transfer coefficient and electron transfer number of controlled step, respectively). Given that $0.3<\alpha<0.7$, it can be concluded that $n=1$, indicates the redox reaction between MP-11and the conductive substrate was a single electron transfer process. The electron transfer rate constant (k_s) of the MP-11 immobilized on the GNPs in the silica cavities on the ITO electrode, is calculated to be ca. 22.6 s^{-1}.

The reproducibility and the stability of this electrode were also tested. The reduced peak currents were measured for 15 times of consecutive cycling at 50 mV/s (after 5 cycles to remove the possible physisorption of MP-11), the result showed a relative standard deviation (RSD) of 7.6%. As for five different electrodes, the RSD was 9.8%. The modified electrode was stored at 4 °C over 20 days and 90% of its original peak current was observed. The long-term property can be attributed to the excellent stability of this electrode.

3.4. Primary application as an hydrogen peroxide biosensor

H_2O_2 is a strong oxidant, yet its electrochemical reduction proceeds with a high overpotential. MP-11 exhibits high

bioelectrocatalytic activities for the reduction of O_2, H_2O_2, organic peroxides and can be applied into biofuel cells and biosensors. In the present case, the MP-11 molecules were immobilized on the functionalized GNPs and assembled inside the silica cavities so that the electrocatalytic reduction of H_2O_2 could occur in a confined volume at the microliter level. It is expected that high sensitivity and low detection limits can be achieved due to the confinement effect, as discussed above. Typical cyclic voltammetric curves of the MP-11/MBA-Au/SiO_2 cavity modified electrode in the absence and presence of H_2O_2 are shown in Fig. 8. The dotted line corresponds to the MP-11/MBA-Au/SiO_2 cavity modified electrode in an argon saturated PBS (curve a). A pair of distinct peaks, corresponding to the redox couple for MP-11, are similar to those in Fig. 6. The presence of H_2O_2 in the solution results in a remarkable increase in the reduction peak current and a shift of the peak potential to less cathodic potentials, accompanied by the disappearance of anodic current (curves b–f). The mechanism of the electrocatalytic process involves the formation of a supervalent ironoxoporphyrin cation radical, followed by two one-electron reduction reactions [44].

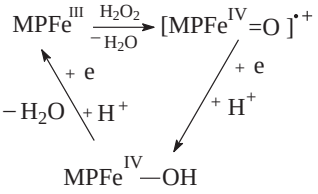

An increase in the concentration of H_2O_2 gives rise to the catalytic current increasing at the same time; moreover, there is a linear relationship between the catalytic current and H_2O_2 concentration, with the linear regression equation expressed as $y=0.2107x+11.041$ ($r=0.998$, $n=19$), when the range of linearity is described from 2×10^{-6} to 6×10^{-4} M. The lowest detectable limit was 6×10^{-7} M ($S/N=3$), which is lower than that of MP-11 immobilized on carbon nanotubes modified Pt microelectrodes [40] and entrapped in lipid membrane [45]. Table 1 compares the surface coverage, the range of linearity and the detection limit of present method with some other reports on hydrogen peroxide biosensor based on MP-11. In addition, this MP-11 electrode exhibited a very rapid response to the changes in H_2O_2 concentration, the steady-state current being reached in 6 s upon successive 1×10^{-5} M H_2O_2 additions. To perform a comparison,

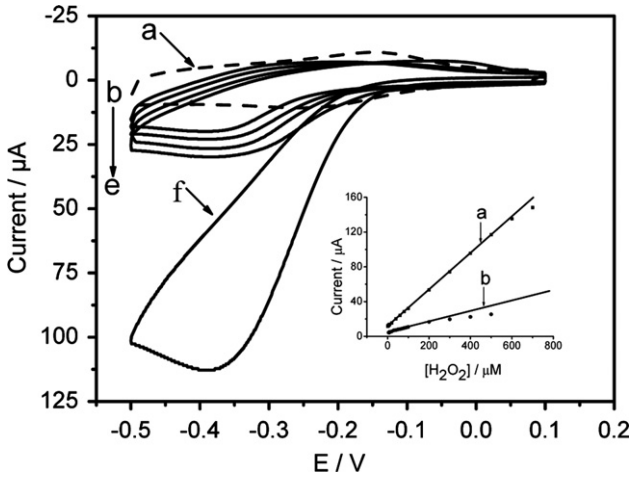

Fig. 8. Cyclic voltammetric curves of MP-11 modified electrode in pH 7.0 PBS (a) without H_2O_2, (b) with 2×10^{-5} M, (c) 3×10^{-5} M, (d) 4×10^{-5} M, (e) 5×10^{-5} M and (f) 4×10^{-4} M H_2O_2 at scan rate 100 mV/s. Inset: calibration curve of electrocatalytic current vs. H_2O_2 concentration (a) with and (b) without microcavities modified at scan rate 100 mV/s.

Table 1
Electrocatalytical properties of MP-11 modified electrodes.

Electrode preparation	Range of linearity (μM)	Detection limit (μM)	Surface coverage ($\times10^{-10}$ mol/L)
Proposed electrode in this paper	2–600	0.6	1.34
Entrapped in lipid membrane [45]	20–2400	0.8	–
Immobilized on carbon nanotubes [40,46]	3.3–38.4	0.7	8.4
Phospholipid functionalized graphene [47]	2–450	0.72	–
In chitosan embedeled gold nanoparticles [48]	1–7	0.27	3.5
Nano-ZnO/MP-11/ pyrolytic graphite [4]	1–700	0.3	3.5

a plate ITO electrode was fabricated with electrodeposited GNPs but without silica cavities. The GNPs were functionalized with the MP-11 molecules through the MBA-linker in a similar manner as described above. The electrocatalytical ability of the electrode was also measured. Although the catalytic current was also linearly proportional to the H_2O_2 concentration, the range of linearity was limited to the range from 1×10^{-5} to 2×10^{-4} M, which is much narrow than that of the silica microcavities modified electrode. Besides, the limit of detection was estimated as only ca. 5×10^{-6} M. Therefore, the micro-sized silica cavity array structure could play an important role in the wide linear range and fast response of these modified electrodes. The modification of the cavity array structure on the electrode surface means that the electrochemical reaction only takes place inside each cavity. That is, the cavities on the electrode generate an array of "soft" microelectrodes. In the present case, the diameter of the cavities is ~2 μm, determined by the size of the templating PS spheres. Very small current would yield in each cavity due to the small effective area for the electrochemical reaction. Because of the edge effect of each cavity with a confined volume, the semispherical diffusion layer and a steady diffusion limited current for the electrochemical reaction could be rapidly achieved inside the cavities.

4. Conclusions

Two dimensional ordered silica cavities were successfully constructed on an ITO electrode. The electrochemical reaction was confined inside the cavities, leading to the electrodeposition of GNPs which was localized at the bottom of the cavities. The MP-11 molecules were subsequently immobilized onto the GNPs inside the cavities through the adsorbed MBA molecules acting as the linker. The electrode had a fast rate of transfer for electrons between the MP-11 molecules, via the GNPs, and the ITO electrode. The confinement effect of the silica cavities endues the electrode with excellent electrocatalytical capability for H_2O_2 reduction, providing a wide linear concentration response range and low limit of detection. Thus, the silica cavity-modified electrode can be applied as a H_2O_2 biosensor.

Acknowledgments

Financial support from the Nature Science Foundation of China (Nos. 20975073, 20873089, 21177067, 21173122), Nature Science Foundation of Jiangsu Province (No.BK2010034) and Scientific

and Technological Innovation Projects of Nantong City (HS2012006) are gratefully acknowledged.

References

[1] G.S. Wilson, M.A. Johnson, Chem. Rev. 108 (2008) 2462–2481.
[2] C. Leger, P. Bertrand, Chem. Rev. 108 (2008) 2379–2438.
[3] A. Yarman, T. Nagel, N. Gajovic-Eichelmann, A. Fischer, U. Wollenberger, F.W. Scheller, Electroanalytical 23 (2011) 611–618.
[4] Y. Astuti, E. Topoglidis, J.R. Durrant, Anal. Chim. Acta 686 (2011) 126–132.
[5] A.H.H. Tanji, F. Lima, S.R. Santos, G. Maia, J. Phys. Chem. C 116 (2012) 18857–18864.
[6] E. Nouri-Nigjeh, A.P. Bruins, R. Bischoff, H.P. Permentier, Analyst 137 (2012) 4698–4702.
[7] K. Saha, S.S. Agasti, C. Kim, X. Li, V.M. Rotello, Chem. Rev. 112 (2012) 2739–2779.
[8] A. Lombardi, F. Nastri, V. Pavone, Chem. Rev. 101 (2001) 3165–3190.
[9] V. Razumas, T. Arnebrant, J. Electroanal. Chem. 427 (1997) 1–5.
[10] M. Li, S. Huang, P. Zhu, L. Kong, B. Peng, H. Gao, Electrochim. Acta 54 (2009) 2284–2289.
[11] K. De Wael, S. De Belder, S. Van Vlierberghe, G. Van Steenberge, P. Dubruel, A. Adriaens, Talanta 82 (2010) 1980–1985.
[12] Y. Liu, A. Offenhausser, D. Mayer, Biosens. Bioelectron. 25 (2010) 1173–1178.
[13] Z.P. Chen, D.M. Sun, Y.M. Zhou, J.Y. Zhao, T.H. Lu, X.H. Huang, C.X. Cai, J. Shen, Biosens. Bioelectron. 29 (2011) 53–59.
[14] L. Gonzalez-Macia, M.R. Smyth, A.J. Killard, Talanta 99 (2012) 989–996.
[15] T. Lötzbeyer, W. Schuhmann, H.-L. Schmidt, J. Electroanal. Chem. 395 (1995) 341–344.
[16] T. Lötzbeyer, W. Schuhmann, E. Katz, J. Falter, H.-L. Schmidt, J. Electroanal. Chem. 377 (1994) 291–294.
[17] L. Jiang, A. Glidle, C.J. McNeil, J.M. Cooper, Biosens. Bioelectron. 12 (1997) 1143–1155.
[18] I. Ivanov, T.R. Vidaković, K. Sundmacher, Electrochem. Commun. 10 (2008) 1307–1310.
[19] L. Gorton, A. Lindgren, T. Larsson, F.D. Munteanu, T. Ruzgas, I. Gazaryan, Anal. Chim. Acta 400 (1999) 91–108.
[20] K. Watts, W. Gattrell, T. Wirth, Beilstein, J. Org. Chem. 7 (2011).
[21] C.E. Reimers, Chem. Rev. 107 (2007) 590–600.
[22] G.S. Wilson, Y.B. Hu, Chem. Rev. 100 (2000) 2693–2704.
[23] A.S. Arico, B.S.P. Bruce, J.-M. Tarascon, W.V. Schalkwijk, Nat. Mater. 4 (2005) 366–377.
[24] M.R. Jones, K.D. Osberg, R.J. Macfarlane, M.R. Langille, C.A. Mirkin, Chem. Rev. 111 (2011) 3736–3827.
[25] E. Menard, M.A. Meitl, Y. Sun, J.-U. Park, D.J.-L. Shir, Y.-S. Nam, S. Jeon, J.A. Rogers, Chem. Rev. 107 (2007) 1117–1160.
[26] Y. Lei, S. Yang, M. Wu, G. Wilde, Chem. Soc. Rev. 40 (2011) 1247–1258.
[27] O.D. Velev, T.A. Jede, R.F. Lobo, A.M. Lenhoff, Chem. Mater. 10 (1998) 3597–3602.
[28] O.D. Velev, T.A. Jede, R.F. Lobo, A.M. Lenhoff, Nature 389 (1997) 447–448.
[29] M.M. Collinson, N. Moore, P.N. Deepa, M. Kanungo, Langmuir 19 (2003) 7669–7672.
[30] M. Kanungo, P.N. Deepa, M.M. Collinson, Chem. Mater. 16 (2004) 5535–5541.
[31] P.N. Bartlett, J.J. Baumberg, S. Coyle, M.E. Abdelsalam, Faraday Discuss. 125 (2004) 117–132.
[32] F. Sun, W. Cai, Y. Li, B. Cao, Y. Lei, L. Zhang, Adv. Funct. Mater. 14 (2004) 283–288.
[33] L. Johnson, D.A. Walsh, J. Mater. Chem. 21 (2011) 7555.
[34] M. Xu, N. Lu, H. Xu, D. Qi, Y. Wang, L. Chi, Langmuir 25 (2009) 11216–11220.
[35] P. Lacroix-Desmazes, J. Guillot, J. Polym. Sci., Part B: Polym. Phys. 36 (1998) 325–335.
[36] T. Wang, X. Hu, X. Qu, S. Dong, J. Phys. Chem. B 110 (2006) 6631–6636.
[37] T.A. Kelf, Y. Sugawara, R.M. Cole, J.J. Baumberg, M.E. Abdelsalam, S. Cintra, S. Mahajan, A.E. Russell, P.N. Bartlett, Phys. Rev. B 74 (2006) 245415.
[38] B.P. Zhang, R.J. Donohoe, J.A. Bailey, J. Raman Spectrosc. 38 (2007) 410–416.
[39] Q. Zhou, J. Zhao, W. Xu, H. Zhao, Y. Wu, J. Zheng, J. Phys. Chem. C 112 (2008) 2378–2381.
[40] M. Wang, F. Zhao, Y. Liu, S. Dong, Biosens. Bioelectron. 21 (2005) 159–166.
[41] H. Zhou, Z. Shi, S. Dong, J. Electroanal. Chem. 443 (1998) 1–3.
[42] E. Laviron, J. Electroanal. Chem. Interfacial Electrochem. 52 (1974) 355–393.
[43] E. Laviron, J. Electroanal. Chem. Interfacial Electrochem. 101 (1979) 19–28.
[44] T. Lötzbeyer, W. Schuhmann, H.-L. Schmidt, Sens. Actuators, B 33 (1996) 50–54.
[45] W. Huang, J. Jia, Z. Zhang, X. Han, J. Tang, J. Wang, S. Dong, E. Wang, Biosens. Bioelectron. 18 (2003) 1225–1230.
[46] M. Wang, Y. Shen, Y. Liu, T. Wang, F. Zhao, B. Liu, S. Dong, J. Electroanal. Chem. 578 (2005) 121–127.
[47] J. Liu, L. Han, T. Wang, W. Hong, Y. Liu, E. Wang, Chem. Asian J. 7 (2012) 2824–2829.
[48] A. Yarman, T. Nagel, N. Gajovic-Eichelmann, A. Fischer, U. Wollenberger, F.W. Scheller, Electroanalysis 23 (2011) 611–618.